In-Situ Investigation of Liquid−Liquid Phase Separation in Polycarbonate/Carbon Dioxide System

Mariko Hatanaka and Hiromu Saito*

Department of Organic and Polymer Materials Chemistry, Tokyo University of Agriculture and Technology, Koganei-shi, Tokyo 184-8588, Japan

Received May 16, 2004; Revised Manuscript Received July 6, 2004

ABSTRACT: We investigated the liquid−liquid phase separation behavior of polycarbonate (PC)/carbon dioxide (CO_2) systems by high fidelity digital microscope and light scattering apparatus equipped with a high-pressure visualized cell. When the PC/CO_2 system was annealed at a temperature above 200 °C, the spherical domain grew and the growth rate decreased with time, suggesting that the liquid−liquid phase separation via nucleation−growth was governed by a diffusion-controlled process under a concentration gradient. In contrast, when the system was annealed at a temperature below 120 °C, a co-continuous two-phase structure with a unique periodicity was detected, and the contrast of the structure became greater with time, suggesting liquid−liquid phase separation via spinodal decomposition. The spinodal decomposition was confirmed by analyzing the time evolution of the Vv light scattering intensity based on the linear theory of Cahn. A spherical porous structure was obtained by quenching and depressurization after the liquid−liquid phase separation via nucleation−growth, while an interconnected, continuously extending porous structure was obtained after the spinodal decomposition.

Introduction

Porous materials made of polymers are used in a wide range of commercial applications because of their properties of low density, high impact resistance, low dielectric constant, and good thermal insulation. A well-known method of producing porous materials is called foaming.[1−3] This method involves saturating the polymer with a pressurized nonreacting gas. When the polymer/gas mixture is quenched into a supersaturated state by depressurization or heating, a large number of gas bubbles nucleate spontaneously and grow with spherical symmetry, resulting in a porous material.[1−9] These nucleation−growth processes are theoretically described by the diffusion-induced growth of a spherical gas bubble surrounded by a thin shell of viscoelastic fluid containing dissolved gas.[10−17] Because of the growth of bubbles with spherical symmetry, closed-cell foams are formed in which spherical air bubbles are entrapped within a continuous polymer phase.[1−9]

Other applications, such as materials for bone substitutes and membranes for filtration or liquid separations, require open cellular materials having a highly interconnected porous structure.[1−3] These materials are usually obtained by methods of phase inversion or thermally induced phase separation.[18] In the former method, a polymer/organic solvent mixture is immersed in a nonsolvent, and the interconnected structure with a polymer-rich phase and a solvent-rich phase is obtained by liquid−liquid phase separation via spinodal decomposition. In the latter method, a single-phase polymer blend is induced to phase separate via spinodal decomposition by a temperature drop, and the partner polymer is extracted by an organic solvent. A disadvantage of both of these methods is the presence of organic solvents during the preparation procedure. Thus, an organic solvent-free process to obtain interconnected porous materials is desirable. Recently, Krause[19,20] and the authors[21] independently found that interconnected porous materials were obtained in polymer/CO_2 systems by annealing under high pressure without the use of an organic solvent. The structure development of polymers under high-pressure CO_2 is helpful in understanding the origin of such interconnected porous structures.

In this paper, we perform in-situ observations of the structure development of a polycarbonate (PC)/CO_2 system at various CO_2 pressures during isothermal annealing after a temperature jump by using a high fidelity digital microscope and light scattering apparatus equipped with a high-pressure visualized cell. The results are discussed in terms of liquid−liquid phase separation via nucleation−growth and spinodal decomposition.

Experimental Section

The polycarbonate (PC) used in this study was supplied by Teijin Limited ($M_w = 1.5 \times 10^4$). To obtain a film specimen with a thickness of ca. 30 μm, the PC pellets were compression-molded between two cover glasses at 210 °C for 3 min and then quickly quenched in a water bath.

In-situ observation of the structure development of PC under high-pressure CO_2 was performed by using a specially designed, custom-made high-pressure visualized cell equipped with two sapphire windows (Taiatsu Techno Co. Ltd.), as described in our previous papers.[22,23] The film specimen (15 mm × 15 mm) was placed on the sapphire window, which is located in the lower part of the cell. After the cell was sealed, high-pressure CO_2 was injected into the cell with a syringe pump (NS-KX-500J, Nihon Seimitsu Kagaku) at room temperature and was held there for 2 h so that the CO_2 would dissolve into the specimen. Then, the temperature was raised to a desired temperature T_a at a rate of 40 °C/min. The pressure of the CO_2 within the cell was monitored with an output pressure transducer and was kept constant during the heating by using a backpressure regulator (SCF-Bpg, Jasco Co., Ltd.). Development of the PC/CO_2 system during the isothermal annealing at T_a was observed under a high fidelity digital microscope (HIROX, MX-5030SZII) equipped above a high-pressure visualized cell. This microscopic system enables real-time observation of the structure with a high resolution of several micrometers. After depressurization and cooling, the

* Corresponding author. E-mail: hsaitou@cc.tuat.ac.jp.

10.1021/ma049036s CCC: $27.50
Published on Web 08/21/2004

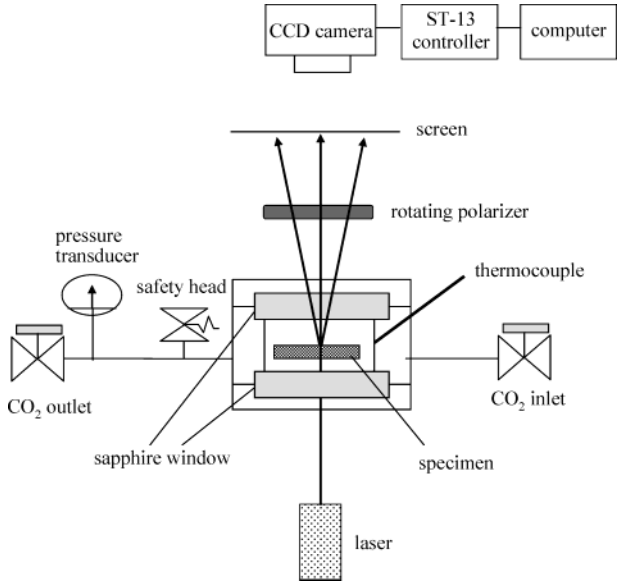

Figure 1. Schematic illustration of a high-pressure visualized cell equipped with a light scattering apparatus.

specimen was removed from the cell for observation with a scanning electron microscope (SEM).

For the qualitative information about the structure development, light scattering apparatus was installed above the high-pressure visualized cell, as shown in Figure 1. A He−Ne laser with a wavelength of 632.8 nm was applied vertically to the film specimen in the cell. The scattered light was passed through an analyzer and then onto a highly sensitive charge-coupled device (CCD) camera with a 512 × 512 pixel sensor having dimensions of 13.3 mm × 8.8 mm (Princeton Instruments, Inc., TE/CDD-512-TKM-1).[24] This sensor provides time-resolved measurements of a two-dimensional angular distribution of scattered light with 512 one-dimensional data points in a time scale of 0.2 s. We employed two optical geometries. One was the Vv geometry in which the optical axis of the analyzer was set parallel to that of the polarizer. The other was the Hv geometry with a perpendicular set of two axes.[25−27] The input data from the CCD camera was digitized by the ST-13X controller and then stored in a personal computer for further analysis.

The structure of the specimen obtained by depressurization and cooling after the isothermal annealing was observed under a SEM (Hitachi S2100A). For SEM observation, the specimen was fractured in liquid nitrogen and sputter-coated with gold.

Results and Discussion

Porous Structure. Figure 2 shows the SEM micrographs of polycarbonate (PC) obtained by cooling and depressurization after annealing at various temperatures T_a for 1 h under CO_2 of 15 MPa. The porous structure is seen in the micrographs. When T_a was higher than 190 °C, closed cells having spherical pores entrapped within a continuous PC phase were obtained (Figure 2a). The spherical porous structure is familiar in polymeric foams.[1−17] In contrast, a continuously extending porous structure was obtained by annealing at low temperature below 190 °C (Figure 2b,c). The continuously extending structures in Figure 2b,c are quite different from the spherical structure shown in Figure 2a. A fibrillar-shaped PC phase and pores having a size of several micrometers are seen in Figure 2b, while the interconnected structure of the PC phase and pores having a size of several tens of micrometers are seen in Figure 2c. Such an interconnected, continuously extending porous structure is unique. To understand the origin of such porous structures, structure development is discussed the in-situ observation under high-pressure CO_2 in the following paragraphs.

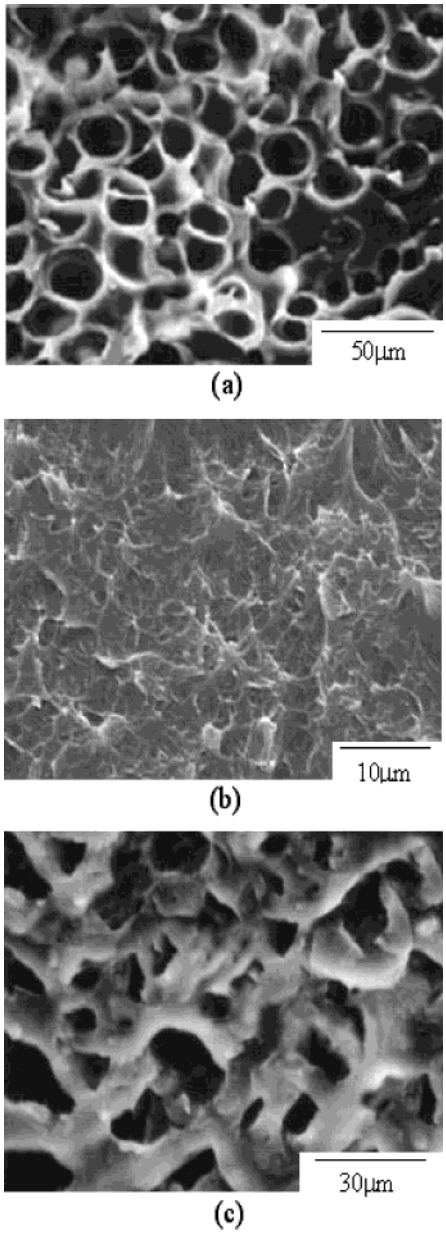

Figure 2. Cellular structure of PC obtained after annealing under CO_2 of 15 MPa at various temperatures: (a) 200, (b) 130, and (c) 120 °C.

Nucleation−Growth. Figure 3 shows the in-situ structure observation of the development of PC under CO_2 of 15 MPa during isothermal annealing at 200 °C after a temperature jump from room temperature. No structure was seen when the CO_2 was dissolved in the PC at room temperature, suggesting that PC and CO_2 are miscible at room temperature in a PC/CO_2 system. After the temperature jump, spherical domains appeared and grew with annealing time (Figure 3a,b). Since the spherical pores are obtained by cooling and depressurization after the annealing (see Figure 2a), the spherical domain in Figure 3 is assigned to the CO_2-rich phase, and the matrix surrounding the domain is assigned to the PC-rich phase. The contrast between the PC-rich phase and the CO_2-rich phase was high and almost unchanged with time. Such structure development is characteristic of the liquid−liquid phase separation via nucleation−growth.[28−30] The nucleation−growth

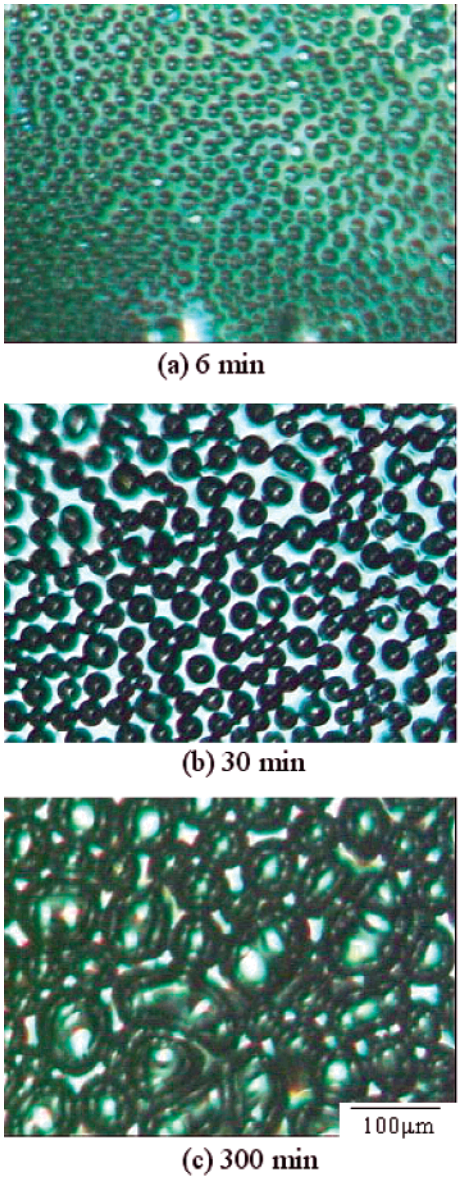

Figure 3. Structure development of PC/CO_2 system at 200 °C and 15 MPa.

occurs at the CO_2 pressures and temperatures indicated by the open circles in Figure 4. Since the liquid−liquid phase separation occurs by raising the temperature, PC and CO_2 are miscible at low temperatures and tend to phase separate at elevated temperatures, suggesting a lower critical solution temperature (LCST)-type phase behavior.

Neighboring CO_2-rich domains impinged on each other after annealing for more than 200 min. The impinged domains coalesced and the interfaces between these domains disappeared. Because of the coalescence of the domains, the spherical domains changed to large deformed domains having a size of about 100 μm (Figure 3c).

The radius of the spherical domain R was obtained from Figure 3. The time variation of R in the PC/CO_2 system is shown at 15 MPa for various annealing temperatures in Figure 5. Here, R was obtained at the time before the impingement of the neighboring domains. R increases as the annealing time increases. The increase of R becomes larger with a decrease in temperature, suggesting that the growth rate increases as

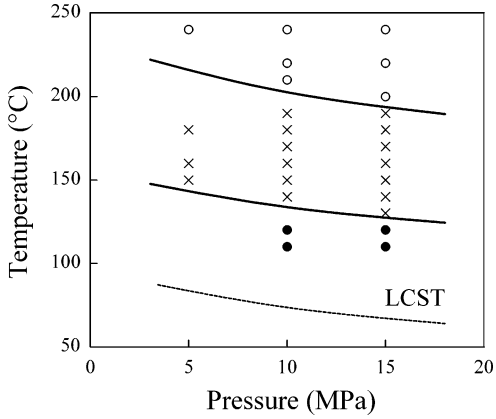

Figure 4. Phase diagram of PC/CO_2 system: (○) nucleation−growth shown in Figure 3, (×) crystallization suggested by Hv light scattering studies,[62] (●) spinodal decomposition shown in Figure 8. The symbols represent temperature and pressure of the experiments made in this work. Broken line is virtual LCST line suggested from eq 4 and Figure 10.

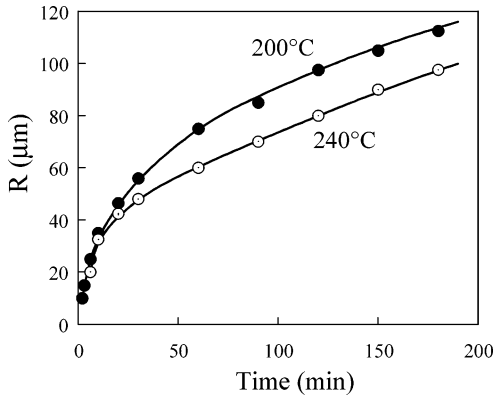

Figure 5. Time variation of the radius of the spherical domain in the PC/CO_2 system at 15 MPa.

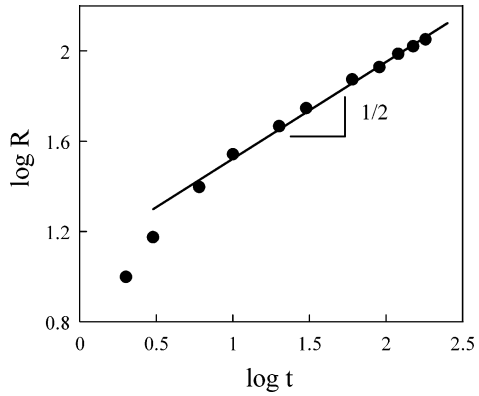

Figure 6. Plot of log R vs log t to analyze the kinetics of the nucleation and growth in PC/CO_2 system at 15 MPa and 200 °C.

the temperature decreases. The interesting result here is the nonlinear growth of the domain; i.e., the increase of R becomes smaller with time t.

As shown in Figure 6, plots of log R vs log t for 200 °C were obtained from Figure 5. The plots yield a straight line after $t = 6$ min (log $t = 0.78$). From the slope of the straight line, R is proportional to the square root of time, $R \propto t^{1/2}$. This suggests that the growth kinetics of the nucleation−growth are governed by a diffusion-controlled process under a concentration gradient formed near the growth front of the CO_2-rich domain, as schematically shown in Figure 7.

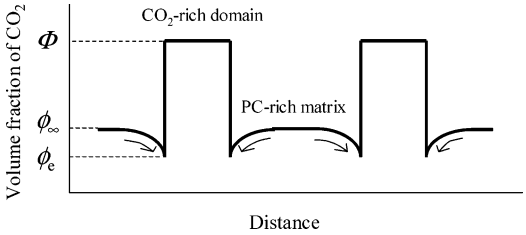

Figure 7. Schematic illustration of concentration profile for diffusion-controlled process.

According to the kinetic theory of Cahn, the growth rate of the domain governed by a diffusion-controlled process is described by[31]

$$R = [2(\phi_\infty - \phi_e)D/\Phi]t^{1/2} \quad (1)$$

where ϕ_∞ is the volume fraction of the CO_2 at a point far from the growth front, ϕ_e is the equilibrium volume fraction at the growth front of the CO_2-rich domain, Φ is the volume fraction of the CO_2 in the CO_2-rich domain, and D is the diffusion coefficient. This may explain $R \propto t^{1/2}$, which is indicated in Figure 6.

As demonstrated in Figure 5, the growth rate increases with decreasing temperature. According to eq 1, the growth rate increases when $(\phi_\infty - \phi_e)$ and D become larger. ϕ_∞ becomes larger with a decreasing temperature because of the increase in the solubility of CO_2 in PC,[32−36] while D becomes larger with increasing temperature. Thus, the increase of the growth rate with decreasing temperature may be ascribed to the large contribution of $(\phi_\infty - \phi_e)$ to the growth of the CO_2-rich domain.

Spinodal Decomposition. Figure 8 shows the in-situ observation of the structure development of the PC/CO_2 system at a CO_2 pressure of 15 MPa during annealing at 120 °C after the temperature jump from room temperature. A highly interconnected two-phase structure with a unique periodicity was detected (Figure 8a). The shape of the structure is different from the spherical domain shown in Figure 3. The contrast of the two-phase structure is much lower than that observed in Figure 3. These results suggest that the liquid−liquid phase separation shown in Figure 8 is different from the nucleation−growth, and the amplitude of the concentration fluctuation is much smaller than that observed in the nucleation−growth. The contrast became higher with time t as shown by a series of micrographs in Figure 8. The increase in contrast is attributed to the growth of the amplitude of the concentration fluctuation. The size of the two-phase structure was initially constant with time (Figure 8a,b), and then it increased (Figure 8c). Such structure development is characteristic of the liquid−liquid phase separation via spinodal decomposition.[28−30] The spinodal decomposition occurred at the CO_2 pressure and temperature indicated by the closed circles in Figure 4.

Details of the liquid−liquid phase separation can be discussed in terms of the results of the time-resolved light scattering. According to the linear theory of Cahn, time evolution of the light scattering intensity associated with the spinodal decomposition is described by[37−39]

$$I_{Vv}(q,t) \propto \exp[2R(q)t] \quad (2)$$

where q is the scattering vector $q = (4\pi/\lambda)\sin(\theta/2)$, θ and λ being the scattering angle and the wavelength of light in the specimen, respectively. $R(q)$ is the growth rate of the amplitude of the concentration fluctuation given by

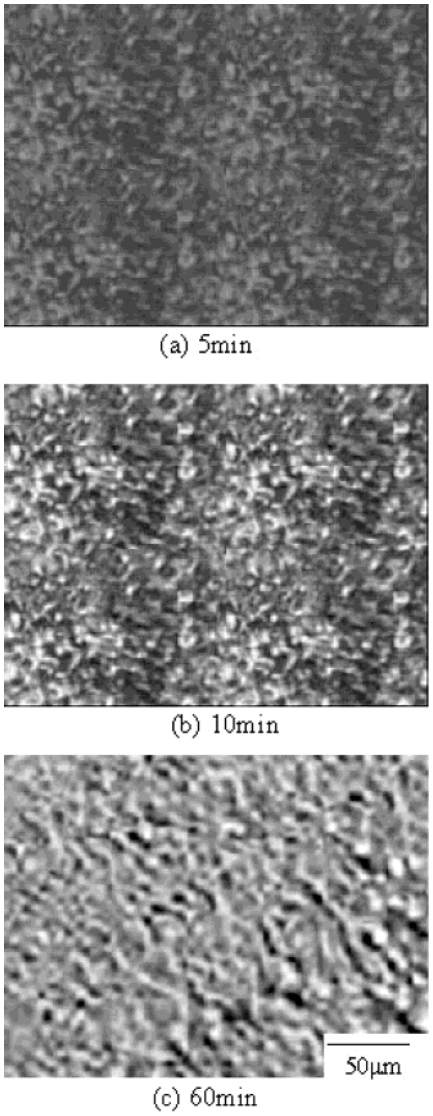

Figure 8. Structure development of PC/CO_2 system at 120 °C and 15 MPa.

$$R(q) = -Mq^2(\partial^2 f/\partial\phi^2 + 2\kappa q^2) \quad (3)$$

where f is the local free energy of the system, ϕ is the volume fraction, κ is the concentration-gradient energy coefficient, and M is the mobility coefficient.

Figure 9 shows the change of the Vv light scattering intensity I at various scattering vectors q's with annealing time t during the structure development indicated in Figure 8. As predicted by eq 2, the exponential increase of I is realized for the liquid−liquid phase separation in the PC/CO_2 system. The exponential character is one of the hallmarks of spinodal decomposition.

According to eq 2, $R(q)$ can be obtained from the slope of ln I vs t plots in Figure 9. The $R(q)$ thus obtained had a maximum at q_m, as shown in Figure 10. Since the periodic distance Λ_m is given by $\Lambda_m = 2\pi/q_m$, the result suggests that the concentration fluctuation having periodic distance Λ_m grows with time and Λ_m is

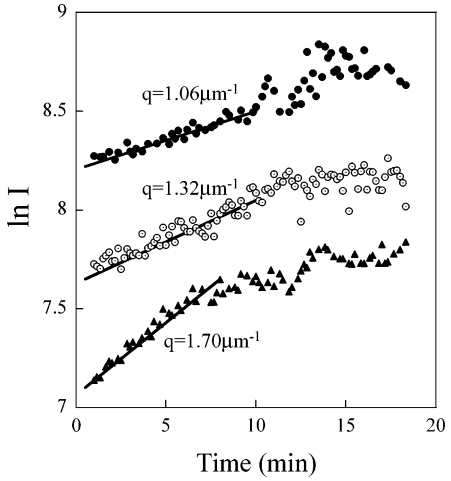

Figure 9. Time variation of scattering light intensity at various q's in the PC/CO_2 system at 15 MPa and 120 °C.

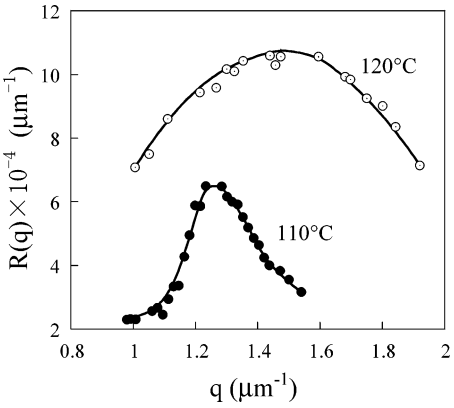

Figure 10. $R(q)$ spectra in the PC/CO_2 system at 15 MPa for various temperatures.

constant with time. This is another hallmark of spinodal decomposition.

q_m increases with increasing temperature. By the linear theory, q_m is an increasing function of the quench depth $|T_a - T_s|$:[38,39]

$$q_m^2 \propto |T_a - T_s| \tag{4}$$

where T_s is the spinodal temperature and T_a is the annealing temperature. As shown in Figure 10, q_m increased with increasing T_a. In eq 4, q_m increases with increasing T_a by assuming that T_a is higher than T_s. This might support the existing of LCST-type phase diagram at low temperature.

Figure 11 shows the plots of $R(q)/q^2$ vs q^2. As expected from eq 3, $R(q)/q^2$ decreases linearly with q^2. This result also confirms that the development of the two-phase structure shown in Figure 8 is caused by liquid−liquid phase separation via spinodal decomposition. The intercept of $R(q)/q^2$ at $q^2 = 0$ in Figure 11 gives the apparent diffusion coefficient D_{app} given by[39−41]

$$D_{app} = M(\partial^2 f/\partial \phi^2) \tag{5}$$

The D_{app} thus obtained was 8.6×10^{-4} $\mu m^2/s$ at 110 °C and 9.1×10^{-4} $\mu m^2/s$ at 120 °C. Here, the self-diffusion coefficient of the PC (D_{PC}) is much smaller than that of the CO_2 (D_{CO_2}); D_{PC} is 10^{-4} $\mu m^2/s$ and D_{CO_2} is 10^6 $\mu m^2/s$.[36,42−47] Thus, the D_{app} is close to D_{PC}, suggesting that D_{app} is governed by the self-diffusion of

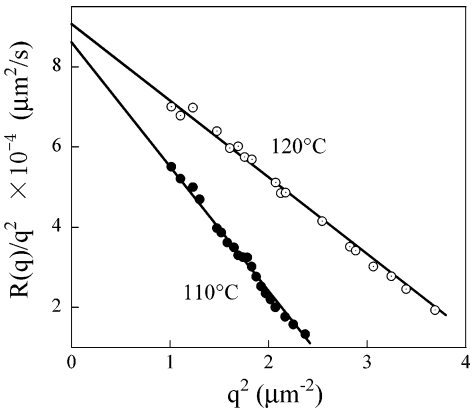

Figure 11. $R(q)/q^2$ vs q^2 plots in the PC/CO_2 system at 15 MPa for various temperatures.

the PC. This may imply that the mobility of the spinodal decomposition is explained by the slow-mode theory in which the mutual diffusion for the spinodal decomposition is mostly governed by the slower moiety. According to the slow-mode theory, the mobility coefficient M in the PC/CO_2 system may be given by[48−51]

$$M \propto \left(\frac{\phi_{PC}}{D_{CO_2}} + \frac{\phi_{CO_2}}{D_{PC}}\right)^{-1} \tag{6}$$

On the other hand, $(\partial^2 f/\partial \phi^2)$ is described by[38−40]

$$\partial^2 f/\partial \phi^2 \propto |T_a - T_s| \tag{7}$$

From eqs 5−7, D_{app} is given by

$$D_{app} \propto \left(\frac{\phi_{PC}}{D_{CO_2}} + \frac{\phi_{CO_2}}{D_{PC}}\right)^{-1} |T_a - T_s| \tag{8}$$

Since ϕ_{CO_2} decreases,[32−36] D increases,[52−54] and $|T_a - T_s|$ increases with increasing temperature, eq 8 can explain the increase of D_{app} with the temperature demonstrated in Figure 11.

The structure change by liquid−liquid phase separation was stopped after a long annealing period when the specimen was annealed at a low temperature. This might be ascribed to the increase of T_g during spinodal decomposition. When the CO_2 is absorbed into PC, T_g of the PC decreases by the plasticizing effect[55−58] and liquid−liquid phase separation occurs despite the lower temperature below T_g of neat PC. As spinodal decomposition proceeds, the concentration of the PC increases in the PC-rich region by increasing the amplitude of the concentration fluctuation and T_g in the PC-rich region is elevated. When T_g in the PC-rich region reaches a temperature above the annealing temperature, the PC-rich phase is vitrified and spinodal decomposition is stopped. This might freeze the interconnected two-phase structure shown in Figure 8 and prevent the coarsening of the structure during depressurization, so that the interconnected, continuously extending porous structure shown in Figure 2c is obtained.

Conclusion

The in-situ observation of the structure development by a high fidelity digital microscope and light scattering revealed that liquid−liquid phase separation occurred in a PC/CO_2 system. Spherical domains were obtained

at temperatures above 190 °C by nucleation−growth. Conversely, highly interconnected two-phase structure was obtained by spinodal decomposition at temperatures below 120 °C. Spinodal decomposition was confirmed by analyzing the time-resolved light scattering results, and the existence of the LCST was suggested. The conditions of the liquid−liquid phase separation observed in this work are summarized in Figure 4. At temperatures between 120 and 190 °C, crystallization of PC occurs, as demonstrated in refs 59 and 60. The Hv and Vv light scattering studies revealed that crystallization of PC and the liquid−liquid phase separation occurred simultaneously at the CO_2 pressure and temperature indicated by the crosses in Figure 4.[61] The competitive progress of the crystallization and liquid−liquid phase separation may cause the fibrillar-shaped PC phase and continuously extending pore shown in Figure 2b. Because the various types of liquid−liquid phase separations occurred at different temperatures and CO_2 pressures, various porous structures were obtained by depressurization and cooling after the liquid−liquid phase separation.

References and Notes

(1) Klempner, D., Frisch, K. C., Eds. *Handbook of Polymeric Foams and Foam Technology*; Hanser Publishers: Munich, 1991.
(2) Khemani, K. C., Ed. *Polymeric Foams, Science and Technology*; American Chemical Society; Washington, DC, 1997.
(3) Kazarian, S. G. *Polym. Sci., Ser. C* **2000**, *42*, 78.
(4) Kumar, V.; Suh, N. P. *Polym. Eng. Sci.* **1990**, *30*, 1323.
(5) Goel, S. K.; Beckman, E. J. *Polym. Eng. Sci.* **1994**, *34*, 1137.
(6) Parks, L. K.; Beckman, E. J. *Polym. Eng. Sci.* **1996**, *36*, 2417.
(7) Arora, K. A.; Lesser, A. J.; McCarthy, T. J. *Macromolecules* **1998**, *31*, 4614.
(8) Stafford, C. M.; Russell, T. P.; McCarthy, T. J. *Macromolecules* **1999**, *32*, 7610.
(9) Krause, B.; Mettinkhof, R.; van der Vegt, N. F. A.; Wessling, M. *Macromolecules* **2001**, *34*, 874.
(10) Rosner, D. E.; Epstein, M. *Chem. Eng. Sci.* **1972**, *27*, 69.
(11) Rutton, D. P. *Chem. Eng. Sci.* **1980**, *35*, 2352.
(12) Amon, M.; Denson, C. D. *Polym. Eng. Sci.* **1984**, *24*, 1026.
(13) Amon, M.; Denson, C. D. *Polym. Eng. Sci.* **1986**, *26*, 255.
(14) Arefmanesh, A.; Advani, S. G.; Michaelides, E. E. *Polym. Eng. Sci.* **1990**, *30*, 1330.
(15) Arefmanesh, A.; Advani, S. G. *Rheol. Acta* **1991**, *30*, 274.
(16) Ramesh, N. S.; Rasmussen, D. H.; Campbell, G. A. *Polym. Eng. Sci.* **1991**, *31*, 1657.
(17) Arefmanesh, M.; Advain, S. G. *Polym. Eng. Sci.* **1995**, *35*, 252.
(18) Porter, M. C. *Handbook of Industrial Membrane Technology*; Noyes Publications: Westwood, NJ, 1990.
(19) Krause, B.; Sijbesma, H. J. P.; Münüklü, P.; van der Vegt, N. F. A.; Wessling, M. *Macromolecules* **2001**, *34*, 8792.
(20) Krause, B.; Diekmann, K.; van der Vegt, N. F. A.; Wessling, M. *Macromolecules* **2002**, *35*, 1738.
(21) Hatanaka, M.; Saito, H. *Proceeding of the Japan Society of Polymer Processing '01 Symposium*, P13: Yonezawa, Japan, 2001.
(22) Oda, T.; Saito, H. *J. Polym. Sci., Part B: Polym. Phys.* **2004**, *42*, 1565.
(23) Teramoto, G.; Oda, T.; Saito, H.; Sano, H.; Fujita, Y. *J. Polym. Sci., Part B: Polym. Phys.* **2004**, *42*, 2738.
(24) Lee, C. H.; Saito, H.; Inoue, T. *Macromolecules* **1993**, *26*, 6566.
(25) Haudin, J. M. In *Optical Properties of Polymers*; Meeten, G. H., Ed.; Elsevier Applied Science Pub.: London, 1986.
(26) Saito, H.; Inoue, T. In *Polymer Characterization Techniques and Their Application to Blends: Light and X-ray Scatterings*; Simon, G. P., Ed.; Oxford University Press: Washington, DC, 2003.
(27) Okada, T.; Saito, H.; Inoue, T. *Macromolecules* **1992**, *25*, 1908.
(28) *Polymer Blend*; Paul, D. R., Newman, S., Eds.; Academic Press: New York, 1978.
(29) Olabishi, O.; Robeson, L. M.; Shaw, M. T. *Polymer−Polymer Miscibility*; Academic Press: New York, 1979.
(30) Utraki, L. A. *Polymer Alloys and Blends*; Hanser: Munich, 1989.
(31) Cahn, J. W. In *Crystal Growth*; Peiser, H. S., Ed.; Pergamon: New York, 1967.
(32) Koros, W. J.; Paul, D. R.; Rocha, A. A. *J. Polym. Sci.* **1976**, *14*, 687.
(33) Fleming, G. K.; Koros, W. J. *Macromolecules* **1986**, *19*, 2285.
(34) Wissinger, R. G.; Paulaitis, M. E. *J. Polym. Sci., Polym. Phys. Ed.* **1987**, *25*, 2497.
(35) Sato, Y.; Talolawa, T.; Takishima, S.; Masuoka, H. *J. Supercrit. Fluid* **2001**, *19*, 187.
(36) Tang, M.; Du, T.-B.; Chen, Y.-P. *J. Supercrit. Fluid* **2004**, *28*, 207.
(37) Cahn, J. W. *J. Chem. Phys.* **1965**, *42*, 93.
(38) Izumitani, T.; Hashimoto, T. *J. Chem. Phys.* **1985**, *83*, 3694.
(39) Lee, C. F.; Saito, H.; Goizueta, G.; Inoue, T. *Macromolecules* **1996**, *29*, 4274.
(40) Hashimoto, T.; Kumaki, J.; Kawai, H. *Macromolecules* **1983**, *16*, 641.
(41) Merfeld, G. D.; Paul, D. R. *Polymer* **2000**, *41*, 649.
(42) Timmerhaus, K. D.; Drickramer, H. G. *J. Chem. Phys.* **1951**, *19*, 1242.
(43) Bachus, R.; Kimmich, R. *Polymer* **1983**, *24*, 964.
(44) Tirrell, M. *Rubber Chem. Technol.* **1984**, *57*, 523.
(45) Blum, F.; Durairaj, B.; Padmanabhn, A. S. *J. Polym. Sci., Polym. Phys. Ed.* **1986**, *24*, 493.
(46) Etesse, P.; Zega, J. A.; Kobayashi, R. *J. Chem. Phys.* **1992**, *97*, 2022.
(47) Kim, E.; Kramer, E. J.; Osby, J. O. *Macromolecules* **1995**, *28*, 1979.
(48) Brochard, F.; Jouffroy, J.; Levinson, P. *Macromolecules* **1983**, *16*, 1638.
(49) Kramer, E. J.; Green, P.; Palmstrom, C. J. *Polymer* **1984**, *25*, 473.
(50) Flory, G.; Cohen, C. *J. Polym. Sci., Polym. Phys. Ed.* **1987**, *25*, 2027.
(51) Hess, W.; Nagele, G.; Akcasu, A. Z. *J. Polym. Sci., Polym. Phys. Ed.* **1990**, *28*, 2233.
(52) Klein, J.; Briscoe, B. J. *Proc. R. Soc. London A* **1979**, *365*, 53.
(53) Wessling, M.; Borneman, Z.; Van Den Boomgaard, Th. *J. Appl. Polym. Sci.* **1994**, *53*, 1497.
(54) Poulsen, L.; Klinger, M.; Eldrup, M.; Sommer-Larsen, P.; Ogilby, P. R. *Macromolecules* **2003**, *36*, 7189.
(55) Chow, T. S. *Macromolecules* **1980**, *13*, 362.
(56) Chiou, J. S.; Barlow, J. W.; Paul, D. R. *J. Appl. Polym. Sci.* **1985**, *30*, 2633.
(57) Wissinger, R. G.; Paulaitis, M. E. *J. Polym. Sci., Part B: Polym. Phys.* **1987**, *25*, 2497.
(58) Condo, P. D.; Sanchez, I. C.; Panayiotou, C. G.; Johnston, K. P. *Macromolecules* **1992**, *25*, 6119.
(59) Chiou, J. S.; Barlow, J. W.; Paul, D. R. *J. Appl. Polym. Sci.* **1985**, *30*, 3911.
(60) Beckman, E.; Porter, R. S. *J. Polym. Sci., Part B: Polym. Phys.* **1987**, *25*, 1511.
(61) Hatanaka, M.; Saito, H., manuscript in preparation.

MA049036S